CRITICAL ANALYSIS OF POWDER FLOW BEHAVIOUR OF DIRECTLY COMPRESSIBLE COPROCESSED EXCIPIENTS

*[1]Salim, I., [2]Khalid, G. M., [3]Wada, A. S., [4]Danladi, S., [5]Kurfi F. S. and [6]Yola U. A.

[1]Department of Pharmaceutics and Pharmaceutical Technology, College of Natural and Pharmaceutical Sciences, Bayero University, PMB 3011, Kano, Nigeria

[2] Department of Pharmaceutics, UCL School of Pharmacy, University College London, 29-39 Brunswick Square, London WC1N 1AX, UK

[3]Department of Pharmacology and Therapeutics, Bayero University, PMB 3011 Kano, Nigeria

[4]Department of Pharmaceutical and Medicinal Chemistry, Bayero University, PMB 3011 Kano, Nigeria

[5]Department of Pharmaceutics and Pharmaceutical Microbiology, Kaduna State University, Nigeria

[6]Department of Pharmaceutical Microbiology and Biotechnology, Bayero University, Kano, Nigeria

*Corresponding authors' email: silyasu.pht@buk.edu.ng Phone: +2347063323898
ORCID: 0000-0002-6961-5703

ABSTRACT

The aim of this pre-formulation study was to adopt simple linear regression modelling and correlation statistics to understand the associations between pharmacopoeial powder test methods using datasets generated from five commercial brands of directly compressible excipients with a specific focus to inferential implications in formulation design. Powder characterization was conducted using protocols defined in Chapter <1174> and <616> of the United States Pharmacopoeia (USP41-NF36). The study adopted a linear regression modelling analytics and correlation statistics using the fitting algorithm of OriginPro® (OriginPro, Version *2021b*, OriginLab Corporation, Northampton, MA, USA). In the results, the modulus of Pearson's product moment correlation coefficient was used to measure the strength of the linear association between test variables and a correlation matrix generated. Strong positive correlation modulus of Hausner's Ratio (HR) with Carr's index (r=+0.999) and static angle of repose (r=+0.932) were evident. Bulk density strongly correlates with tap density in the positive direction (r=+0.911). Tap density also shows a slight negative correlation with HR (r=-0.230), Carr's index (r=-0.228), and static angle of repose (r==-0.421), while Carr's index strongly correlated with static angle of repose (r=+0.933). In conclusion, modelling bivariate powder flow datasets has provided a powerful but simplistic statistical relationship for characterizing the modulus of association between HR, Carr's index, and static angle of repose of the model excipients useful in preformulation design of pharmaceutical formulations.

Keywords: Coprocessed excipients; Powder flow, Statistical modelling, Simple Linear Regression, Pearson's Correlation, Correlation Matrix

INTRODUCTION

Direct compression tablet technology offers a cost-effective alternative route of manufacturing conventional tablets and specialized drug delivery systems (Armstrong, 2007; Rojas et al., 2012; Wang & Sun, 2021). Relative to granulation technology, direct compression technology utilizes shorter production operations aggregating to minimal risk of product contamination, ease of compliance to current Good Manufacturing Practices guidelines, and net low production costs (Alderborn & Frenning, 2017; Armstrong, 2007). Because most of the active pharmaceutical active ingredients lack the required micromeritic functionality to withstand high-speed compaction, the formulation technology utilizes special form of pharmaceutical powder diluents (excipients) to improve the flow metrics of the powder system (Armstrong, 2007). Consequently, efficient powder flow is a critical requirement of such diluents for efficient and reproducible die filling as well as consistency of unit doses (Alderborn & Frenning, 2017; Salim et al., 2018). The ability to quantitatively assess the tendency of powders to flow, is crucial for design, operation, and quality assurance in many industrial processes involving powders. Similarly, upstream in-process unit operations such as bulk discharge of formulation ingredients from storage bins to mixing vessels, the dynamics of convection, dispersion, and shearing in blending operations, and subsequent transfer of formulation mix into tablet hoppers are all strongly dependant on powder flow properties of the diluents (Armstrong, 2007; Twitchell, 2018).

Preformulation analysis involves critical analysis of powder flow properties (Pérez et al., 2006; Salim et al., 2021). In powder technology, measurements of angle of repose, density ratios (Carr's index and Hausner's ratio) flow rate, and shear cell methods have been used to quantify the magnitude of powder flow (Krantz et al., 2009; Marchetti & Hulme-Smith, 2021; Salehi et al., 2017). For engineering and industrial applications, single test methods are seldom used to adequately characterize powder flow behaviour. Multiple testing methods are quite widely adopted to characterize powder systems (Krantz et al., 2009; Marchetti & Hulme-Smith, 2021). However, due to the extensive variability of the testing methods and stochastic behaviour of powder systems, conflicting results are often inevitable. To overcome this critical concern, it was strongly recommended that multiple testing methods be thoroughly investigated and validated in specific powder applications (Goh et al., 2018; Krantz et al., 2009; Marchetti & Hulme-Smith, 2021).

In the literature, several studies were directed towards comparison of powder test methods. Using linear, non-linear, and polynomial regression analysis a critical analysis of Hall flow rate, Carney flow rate, angle of repose, conditioned bulk density, tapped density, shear test, and fixed funnel angle of

repose of steel metal powders was conducted by Marchetti & Hulme-Smith, 2021. Similarly, a comparison between Jenike shear cell, the Schulze ring shear tester, and the Brookfield powder flow tester was conducted by Salehi et al., 2017. After comparing various static and dynamic techniques for characterising powders, Krantz et al., 2009 came to the conclusion that the best characterization method should be chosen based on its capacity to accurately reproduce the state of stress and powder compaction in a setting that is as close to the powder process condition as possible. The aim of this preformulation research was to adopt simple linear regression modelling and correlation statistics to validate the associations between United States Pharmacopeial powder test methods using datasets generated from five commercial brands of directly compressible excipients with a specific focus to inferential implications in formulation design.

MATERIALS AND METHODS
Materials
The materials evaluated in this study were five directly compressible coprocessed diluents. All excipients were of pharmaceutical grade and have been directly sourced from the manufacturers. The general description of the diluents is given in Table 1. RetaLac®, Cellactose 80®, CombiLac®, and Ludiflash® are directly compressible co-spray dried agglomerates comprising of excipients enlisted in Table 1. Vivapharm® HPMC E50 powder is a Hypromellose 2910 (hydroxypropyl methylcellulose). All excipients were compliant to specific pharmacopoeia(s).

Table 1: Description of the powder materials characterized in the study

Brand name	Lot Number	Composition	Manufacturer	Particle size distribution
RetaLac®	L104394500068782A990	50% Lactose monohydrate/50% Hypromellose	Meggle Group Wasserburg, BG Excipients & Technology, Germany	<63µm NMT 25%, <250 µm NLT 80%
Cellactose80®	L100463318	75% Lactose monohydrate (Ph. Eur.)/25% Powdered cellulose	Meggle Group Wasserburg, BG Excipients & Technology, Germany	<32 µm NMT 20%, <160 µm 35-65%, <250 µm NLT 80%.
CombiLac®	L100064418	70% Lactose monohydrate (ph. Eur.)/10% white native maize starch (Ph. Eur.)/20% Microcrystalline cellulose (Ph. Eur.)	Meggle Group Wasserburg, BG Excipients & Technology, Germany	<32 µm NMT 15%, <160 µm 35-65%, <250 µm NLT 85%.
Ludiflash®	91941247G0	D-Mannitol (84.0-92.0%), Povidone (0.25-0.60%), Polyvinyl acetate (3.5-6.0%), Kollidon® CL-SF (4.0-6.0%), and water (0.5-2.0%)	BASF SE, Ludwigshafen, Germany	> 400 µm maximum 20% < 200 mm maximum 90%, minimum 45% < 63 mm maximum 45%, minimum 15%
VIVAPHARM® HPMC E50 (Hypromellose 2910)	13867/17 x	Hydroxypropyl methyl cellulose (USP, Ph. Eur., JP)	JRS Pharma, GMBH & Co., Germany	

USP: United States Pharmacopoeia, Ph. Eur.: European Pharmacopoeia, JP: Japanese Pharmacopoeia, NMT; Not more than, NLT; Not less than.

Methods
Powder densities were measured as described under Chapter <616> of the United States Pharmacopoeia (USP, 2018). The parameters derived from density measurements were substituted into the relevant equations of powder flow measurement described under Chapter <1174>. The experimental set up for density and angle of repose measurements was schematically depicted in (Figure 1A-C). In this research, five powder flow parameters were determined; Bulk density, Tap density, Hausner's ratio, Carr's index, and Static angle of repose. Simple Linear Fitting was then performed on bivariate datasets to investigate the linear association between the powder variables.
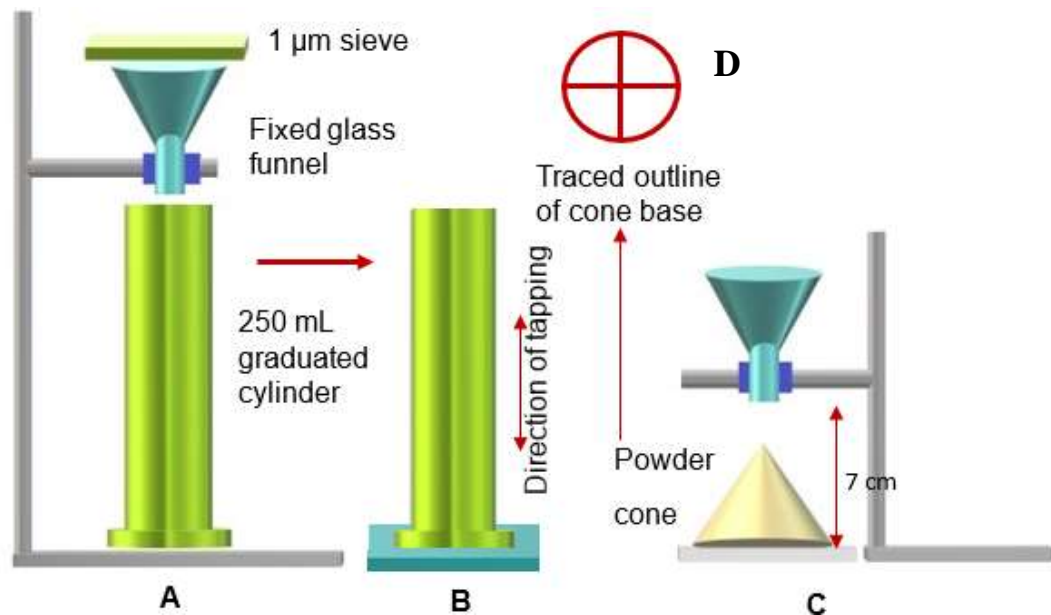
Figure 1: Schematic illustration of standardized United States Pharmacopoeia Method I for measurement of Bulk density (A) and Tap density (B). Experimental set up for static angle of repose (C) and the traced outline of the base of the powder cone depicted by (D).

Bulk density
Bulk density (ρ_b) was determined as the ratio of weight (w) to volume (V_0) of loosely assembled powder particles (Eq. 1) (*Bulk Density and Tapped Density of Powders | USP*, n.d.; USP, 2015). The powder was poured through 1 µm sieve aperture into a glass funnel and down to a 250 mL graduated cylinder (Figure 1A). Necessary precautions were taken to avoid untoward vibrations and excessive stress during powder packing. The cylinder was gently levelled and the nearest graduation read as V_0.

$$\rho_b = \frac{W}{V_0} \qquad (1)$$

Tap density
Tap density (ρ_t) was determined as the weight (W) to volume (V_t) ratio of tapped bed of powder in the 250 mL graduated cylinder (Eq. 2) (*Bulk Density and Tapped Density of Powders | USP*, n.d.). Reference to Figure 1B, V_t was obtained by gently tapping the cylinder at the rate of 150 taps/minute on a cushioned table top in a biaxial direction. The maximal distance between the raised cylinder bas and the surface of the table was maintained at approximately 1.4 cm. Three replicate determinations were conducted.

$$\rho_t = \frac{W}{V_t} \qquad (2)$$

Where V_t represents the final deaerated powder volume following 500 taps.

Carr's index (IC) and Hausner's ratio (HR)
Because the weight of powders for bulk and tap densities measurements were equivalent in most cases, Eq. 3 & 4 were used for Carr's index (IC) and Hausner's ratio (HR) measurements. In exceptional settings, were the initial weights varied, Eq. 5 & 6 were utilized for IC and HR, respectively.

$$IC = \left[\frac{V_0 - V_t}{V_0}\right].100 \qquad (3)$$

$$HR = \frac{V_0}{V_t} \qquad (4)$$

$$IC = \left[\frac{\rho_t - \rho_b}{\rho_t}\right].100 \qquad (5)$$

$$HR = \frac{\rho_t}{\rho_b} \qquad (6)$$

Static angle of repose (AR)
With reference to Figure 1C, the Static angle of repose (α_S) was determined using the fixed funnel method. The funnel was fixed at 90° to the horizontal plane and its tip raised 7 cm away from table surface. Sample of 20 g of powder was carefully packed in the blocked glass funnel. Because all experimental powders were free-flowing, test sample evacuates the funnel under the influence of gravity to form a powder cone. The diameter and hence the radius (R) was obtained from the base of the cone as traced with an ink (Figure 1D). The maximum height (H_{max}) was measured with aid of a 10 cm ruler. The static angle of repose (α_s) was calculated as the inverse of the tangent function (arctangent) of the ratio H_{max} to R (Eq. 7) (Beakawi Al-Hashemi & Baghabra Al-Amoudi, 2018).

$$AR = Arctan\left(\frac{H_{max}}{R}\right) \qquad (7)$$

Linear regression modelling algorithm
Simple linear regression analysis was conducted on paired powder test methods to investigate their linear trend. Simple linear regression was used to verify the relationship between the independent and dependent variables. The null hypothesis (H_o) that there was no linear association between bivariate powder test methods was tested using *t*-test such that β_o or β_1 in Eq. 8 equate to zero if H_o was true. Given a confidence level of α, H_o was rejected when $|t| > t_{\frac{\alpha}{2}}$ and that also that the *p*-value was less than α (Mohr et al., 2022). Pearson product moment correlation coefficient was used to measure the strength of the linear association between test variables. Adjusted coefficient of determination (Adj R-square) was used to determine the regression model's ability to explain the observed association. Statistical significance was considered for *p*<0.05. All the experimental datasets for building the regression model were presented in the supplementary data (Table 2-6). The actual values used were the means of the various replicate experimental determinations. The results presented were based on the linear fitting algorithm of OriginPro® 2021b (OriginPro, Version *2021b*, OriginLab Corporation, Northampton, MA, USA) statistical software. Given that (x_i, y_i) was the bivariate powder flow dataset

where $i = 1, 2, \ldots \ldots n$ and that x and y were the independent and dependent variables, respectively, the linear regression fit was defined by (Mohr et al., 2022; Moser, 1996):

$$y_i = \beta_o + \beta_1 x_i + \varepsilon_i \tag{1}$$

where, the coefficients β_o and β_1 are model parameters and ε_i is a random error whose variance and mean are δ^2 and $E\{\varepsilon_i\}$, respectively. Using the least square estimation method, the sum of n squared deviations (SS) was minimized using Eq. 9 (Angelini, 2019; Origin Help - Algorithms (Linear Regression), n.d.; Ostertagová, 2012).

$$SS = \sum_{i=1}^{n}(Y_i - \beta_0 - \beta_1 X_i)^2 \tag{2}$$

However, the estimated parameters of the linear regression model were given by Eq. 10 & 11.

$$\widehat{\beta_1} = \frac{SXY}{SXX} \tag{3}$$

$$\widehat{\beta_o} = \bar{y} - \widehat{\beta_1}\bar{x} \tag{4}$$

where,

$$\bar{x} = \frac{1}{n}\sum_{i=1}^{n} x_i, \bar{y} = \frac{1}{n}\sum_{i=1}^{n} y_i \tag{5}$$

$$SXY = \sum_{i=1}^{n}(x_i - \bar{x})(y_i - \bar{y}) \tag{6}$$

$$SXX = \sum_{i=1}^{n}(x_i - \bar{x})^2 \tag{7}$$

Consequently, the regression function used to fit the dataset was of the form:

$$\hat{y} = \widehat{\beta_0} + \widehat{\beta_1}x \tag{8}$$

The residual was given by:

$$\tilde{y} = y_i - \hat{y_i} \tag{16}$$

Using (9), the residuals were minimized, and thus the residual sum of squares (RSS) was given by:

$$RSS = \sum_{i=1}^{n}(y_i - \hat{y_i})^2 \tag{9}$$

Table 2: Data for bulk density determination

Excipients	Powder weight (g)		Bulk volume (mL)		Bulk density (g/mL)	
RetaLac®	W_1	44.1	V_{01}	182	ρ_{b1}	0.242
	W_2	44.4	V_{02}	184	ρ_{b2}	0.241
	W_3	44.4	V_{03}	186	ρ_{b3}	0.239
	$\bar{W}$	44.3	$\bar{V_0}$	184	$\overline{\rho_b}$	0.241
	σ_w	0.17	σ_{V_0}	2.00	σ_{ρ_b}	0.002
Ludiflash®	W_1	100.0	V_{01}	216	ρ_{b1}	0.463
	W_2	100.0	V_{02}	214	ρ_{b2}	0.467
	W_3	100.0	V_{03}	216	ρ_{b3}	0.463
	$\bar{W}$	100.0	$\bar{V_0}$	215.3	$\overline{\rho_b}$	0.464
	σ_w	0.00	σ_{V_0}	1.156	σ_{ρ_b}	0.002
Cellactose80®	W_1	100.3	V_{01}	228	ρ_{b1}	0.440
	W_2	100.0	V_{02}	218	ρ_{b2}	0.459
	W_3	100.0	V_{03}	220	ρ_{b3}	0.455
	$\bar{W}$	100.1	$\bar{V_0}$	222	$\overline{\rho_b}$	0.451
	σ_w	0.17	σ_{V_0}	5.292	σ_{ρ_b}	0.010
CombiLac®	W_1	100.6	V_{01}	200	ρ_{b1}	0.503
	W_2	100.2	V_{02}	194	ρ_{b2}	0.516
	W_3	100.0	V_{03}	196	ρ_{b3}	0.510
	$\bar{W}$	100.3	$\bar{V_0}$	196.7	$\overline{\rho_b}$	0.510
	σ_w	0.31	σ_{V_0}	3.055	σ_{ρ_b}	0.007
VIVAPHARM® HPMC	W_1	9.0	V_{01}	21.5	ρ_{b1}	0.419
	W_2	9.1	V_{02}	22	ρ_{b2}	0.414
	W_3	9.0	V_{03}	21	ρ_{b3}	0.429
	$\bar{W}$	9.03	$\bar{V_0}$	21.5	$\overline{\rho_b}$	0.420
	σ_w	0.06	σ_{V_0}	0.500	σ_{ρ_b}	0.008

$\bar{W}$: Mean powder weight, σ_w: Standard deviation of powder weight, $\bar{V_0}$: Mean bulk volume $\overline{\rho_b}$:Mean bulk density

Table 3: Data for tap density determination

Excipients	Powder weight (g)		Tap volume (mL)		Tapped density (g/mL)	
RetaLac®	W_1	44.4	V_{01}	132	ρ_{b1}	0.336
	W_2	44.0	V_{02}	130	ρ_{b2}	0.338
	W_3	44.4	V_{03}	136	ρ_{b3}	0.326
	$\bar{W}$	44.3	$\bar{V_0}$	132.7	$\overline{\rho_b}$	0.334
	σ_w	0.231	σ_{V_0}	3.06	σ_{ρ_b}	0.006
Ludiflash®	W_1	100	V_{01}	162	ρ_{b1}	0.617
	W_2	100	V_{02}	164	ρ_{b2}	0.610
	W_3	100	V_{03}	160	ρ_{b3}	0.625
	$\bar{W}$	100	$\bar{V_0}$	162	$\overline{\rho_b}$	0.617
	σ_w	0.00	σ_{V_0}	2.00	σ_{ρ_b}	0.008
Cellactose80®	W_1	100.3	V_{01}	194	ρ_{b1}	0.517
	W_2	100	V_{02}	192	ρ_{b2}	0.521
	W_3	100	V_{03}	192	ρ_{b3}	0.521
	$\bar{W}$	100.1	$\bar{V_0}$	192.7	$\overline{\rho_b}$	0.520
	σ_w	0.173	σ_{V_0}	1.16	σ_{ρ_b}	0.002

CombiLac®	W_1	100	V_{01}	176	ρ_{b1}	0.568
	W_2	100	V_{02}	170	ρ_{b2}	0.588
	W_3	100	V_{03}	166	ρ_{b3}	0.602
	$\overline{W}$	100	$\overline{V}_0$	170.7	$\overline{\rho_b}$	0.586
	σ_w	0.000	σ_{V_0}	5.03	σ_{ρ_b}	0.017
VIVAPHARM® HPMC	W_1	9	V_{01}	15	ρ_{b1}	0.600
	W_2	9.1	V_{02}	15.5	ρ_{b2}	0.587
	W_3	9	V_{03}	15	ρ_{b3}	0.600
	$\overline{W}$	9.0	$\overline{V}_0$	15.2	$\overline{\rho_b}$	0.596
	σ_w	0.06	σ_{V_0}	0.29	σ_{ρ_b}	0.007

$\overline{W}$: Mean powder weight, σ_w: Standard deviation of powder weight, $\overline{V}_t$: Mean tap volume $\overline{\rho_t}$:Mean tap density

Table 4: Data for Density ratios (Hausner's ratio and Carr's index) determination

Excipients	Hausner's ratio (HR)		Carr's index (IC) (%)	
RetaLac®	HR_1	1.39	IC_1	28
	HR_2	1.40	IC_2	29
	HR_3	1.37	IC_2	27
	$\overline{HR}$	1.39	$\overline{IC}$	28
	σ_{HR}	0.02	σ_{IC}	1
Ludiflash®	HR_1	1.33	IC_1	25
	HR_2	1.30	IC_2	23
	HR_3	1.35	IC_2	26
	$\overline{HR}$	1.33	$\overline{IC}$	25
	σ_{HR}	0.02	σ_{IC}	1
Cellactose80®	HR_1	1.18	IC_1	15
	HR_2	1.14	IC_2	12
	HR_3	1.15	IC_2	13
	$\overline{HR}$	1.15	$\overline{IC}$	13
	σ_{HR}	0.02	σ_{IC}	2
CombiLac®	HR_1	1.13	IC_1	11
	HR_2	1.14	IC_2	12
	HR_3	1.18	IC_2	15
	$\overline{HR}$	1.15	$\overline{IC}$	13
	σ_{HR}	0.03	σ_{IC}	2
HPMC (VIVAPHARM)	HR_1	1.43	IC_1	30
	HR_2	1.42	IC_2	30
	HR_3	1.40	IC_2	29
	$\overline{HR}$	1.42	$\overline{IC}$	29
	σ_{HR}	0.02	σ_{IC}	1.0

HR: Hausner's ratio, $\overline{HR}$: Mean of Hausner's ratio, σ_{HR}: Standard deviation of HR, IC: Carr's index, $\overline{IC}$: Mean of Carr's index. The subscripts 1,2, & 3 represent the first, second, and the third experimental runs, respectively. HR and IC values were calculated from Table 1 and Table 2.

Table 5: Data for static angle of repose measurement

S/No.	Excipient	Height of the cone			Diameter of the cone			$h_1/0.5d_1$	$h_2/0.5d_2$	$h_3/0.5d_3$
		h_1	h_2	h_3	d_1	d_2	d_3			
1	Ludiflash®	2	2	1.9	8.03	8.2	8.17	0.498	0.488	0.465
2	Combilac ®	1.6	1.4	1.5	8.5	8.73	8.77	0.376	0.321	0.342
3	VIVAPHARM HPMC ®	1.8	2	1.9	6.7	6.5	6.85	0.537	0.616	0.555
4	Cellactose 80®	0.9	0.9	0.9	7.1	6.96	7.1	0.254	0.259	0.254
5	RetaLac®	2.5	2.3	2.5	7.36	7.03	7.1	0.679	0.654	0.704

Height of powder cone (h), Diameter of powder cone (d). Refer to Figure 1C & Figure 1D.

Table 6: Data for static angle of repose measurement (derived from Table 5)

S/No.	Excipient	$\tan\alpha_s$ (h1/0.5d1)	$\tan\alpha_s$ (h2/0.5d2)	$\tan\alpha_s$ (h3/0.5d3)	Static angle of repose (α_s) in °			α_{smean}	α_s std
					α_{s1}	α_{s2}	α_s		
1	Ludiflash®	0.462	0.454	0.435	24.80	24.41	23.53	24.25	0.655
2	Combilac ®	0.360	0.310	0.330	19.80	17.24	18.24	18.43	1.29
3	VIVAPHARM HPMC ®	0.493	0.551	0.506	26.25	28.88	26.86	27.33	1.38
4	Cellactose 80®	0.248	0.253	0.248	13.94	14.20	13.94	14.03	0.149
5	RetaLac®	0.597	0.579	0.614	30.83	30.09	31.53	30.82	0.721

Height of powder cone (h), Diameter of powder cone (d). Refer to Figure 1C & Figure 1D, α_{smean}: Mean Static angle of repose, α_s std: Standard deviation.

RESULTS AND DISCUSSION

Pharmaceutical powder systems display non-Newtonian rheological dynamics and therefore must be acted upon by intrinsic and extrinsic factors to possess the driving force necessary for fluidization (Lu et al., 2023). Although powders are widely considered as solid state of matter, they share certain kinetic similarities with fluids when acted upon by considerable stress which fluidizes static powder bed and initiates flow. Characterization and modelling of powder flow patterns are difficult owing to the stochastic nature of bulk powders. For instance, the general powder flow characteristics of the experimental diluents is presented in the parallel coordinate plot. The plot provided only a descriptive statistic of the flow indices with no specific trend (Figure 2). Similarly, the raw data of powder flow metrics shown in Table 2-6 were also devoid of meaningful inference for practical use. For practical applications, interpretation of the real (true) associations of the flow metrics would aid rational design of unit operations in tablet formulation development by direct compression. In this research we adopted regression analysis to inferentially provide a better understanding of the flow behaviour and the relationships between the test methods. Such inferences are very useful in early formulation development and prevents false interpretation of powder flow datasets.
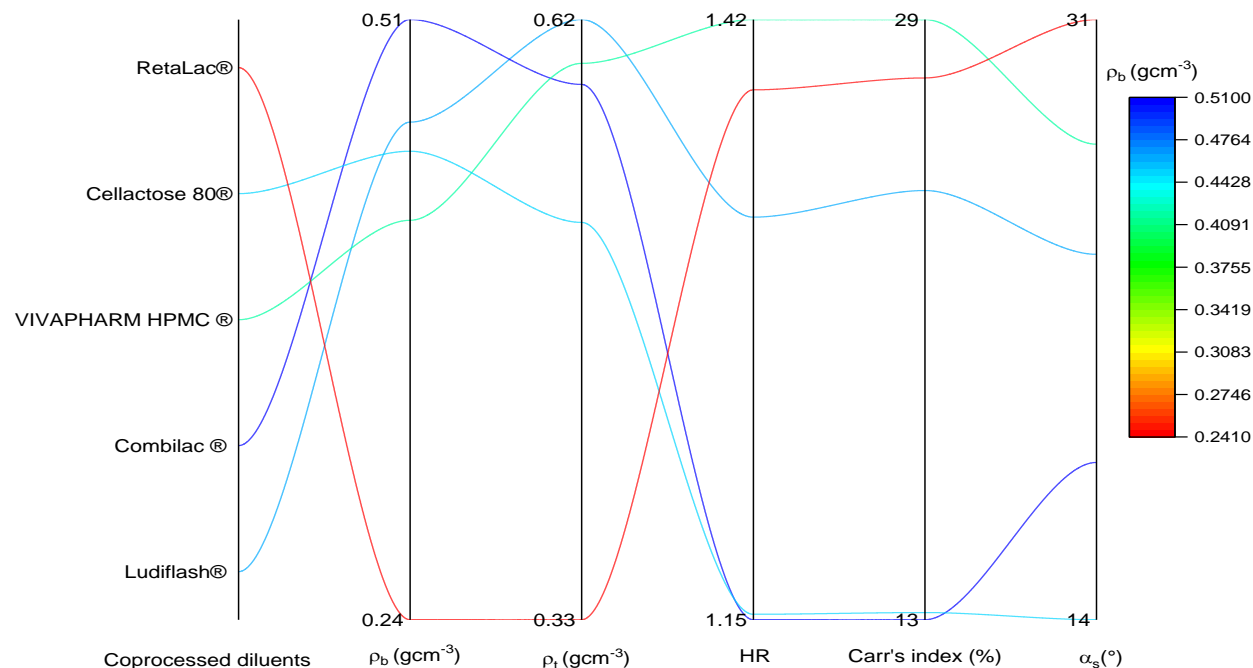
Figure 2: Parallel coordinates plot. General description of flowability parameters on a set of numeric variables. Each vertical bar represents a flowability parameter with its own scale.

Linear association between the test methods

Here we discussed five important associations between the test methods.

i. Linear association between bulk density (pb) and tap density (pt)

ii. Linear association between tap density and Hausner's ratio (HR)

iii. Linear association between Carr's index and Hausner's ratio

iv. Linear association Carr's index and static angle of repose

v. Linear association between Hausner's ratio (HR) and static angle of repose

The linear association between bulk and tap density was presented in Figure 3. The bulk density consists of the volume occupied by the bulk powder material together with its inter- and intra-particulate voids (Amidon et al., 2017). The bulk density is particularly dependent on the packing geometry attained due to random settling of the particles. The tapped density is essentially tapped bulk density attained by successive tapping to constant volume. Both densities could provide an indirect measure of powder flow. Denser materials tend to flow better under the influence of gravity than less. While the true values of the respective densities could differ considerably, there exist a strong correlation between the bulk and tap densities. This points to similar bulk particulate rearrangement and volume reduction propensities of the diluents used in the study. The Pearson's r indicates the strength of the linear association between the dependent (ρ_b) variable and the independent variable (ρ_t). Accordingly, there was positive correlation between ρ_b and ρ_t (Pearson's r=0.910) (Figure 3). The Adjusted R-Square measures the ability of the model to explain the relation between the variables. Tap density has been defined as the ratio of weighted powder sample to its deaerated volume. The Hausner's ratio is otherwise called density ratio obtained by dividing the tap density with bulk density or bulk volume by tap volume. In this research, we found no correlation between these variables (Figure 4).

y = (-0.00881603) + (0.804107) * x	
	ρb (g/mL)
Pearson's r	0.91075
Adj. R-Square	0.77263
Intercept	-0.00882 ± 0.11369
Slope	0.80411 ± 0.2105
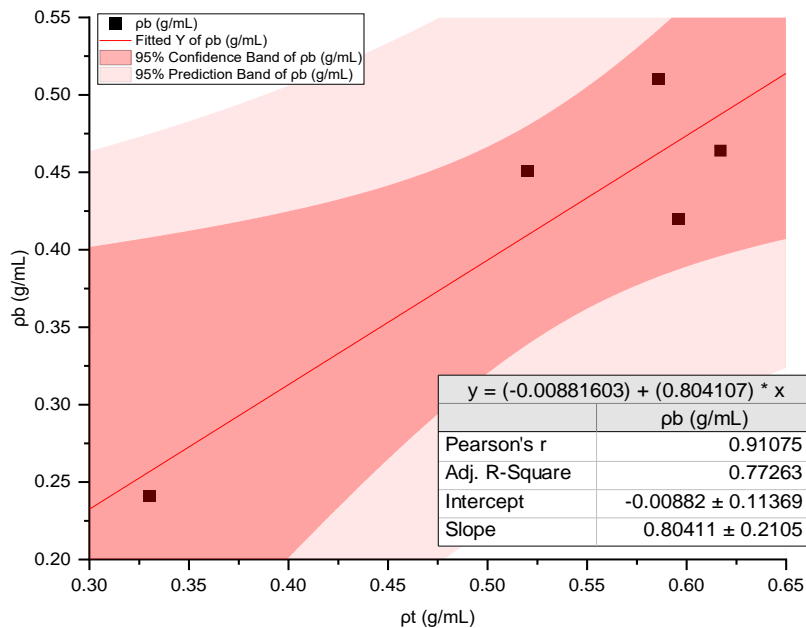
Figure 3: Correlation between bulk density (pb) and tap density (pt). The linear fit is indicated by the straight line followed by 95% confidence band of bulk density (denser band) and 95% prediction bands of bulk density (lighter band), respectively.

y = (0.801362) + (-0.211003) * x	
	ρt (g/mL)
Pearson's r	-0.23027
Adj. R-Square	-0.26263
Intercept	0.80136 ± 0.6652
Slope	-0.211 ± 0.51482
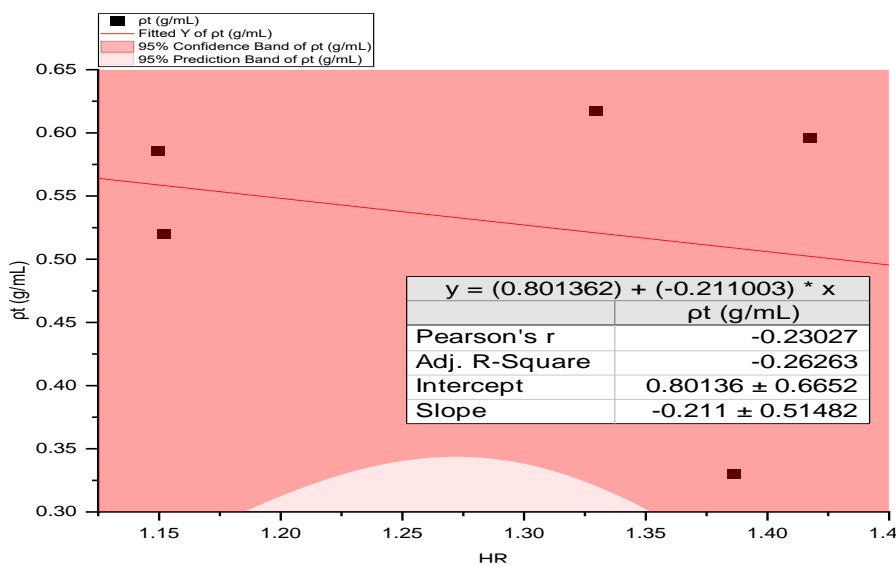
Figure 4: Correlation between tap density and Hausner's ratio. The linear fit is indicated by the straight line followed by 95% confidence and prediction bands, respectively.
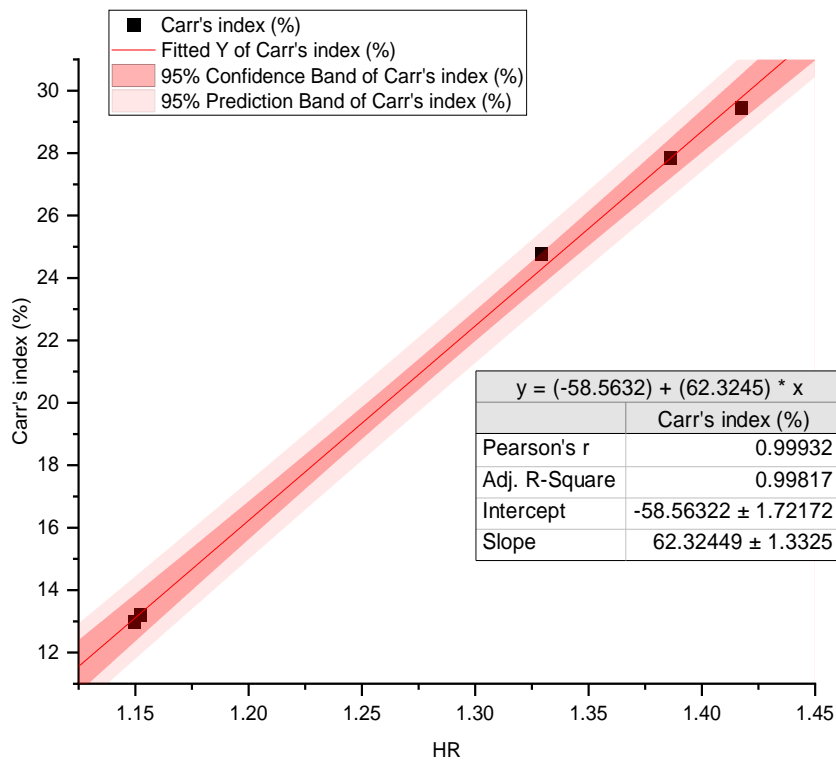
Figure 5: Correlation between Carr's index and Hausner's ratio. The linear fit is indicated by the straight line followed by 95% confidence and prediction bands, respectively.

For the Carr's index and Hausner's ratio there was strong positive correlation. This was the highest correlation attained among all the paired test methods Figure 5. Hausner discovered a correlation between interparticulate friction and the density ratio (Eq. 6 and Eq. 4). As a result, he was able to show that the ratio accurately predicted powder flow. He demonstrated that more cohesive, less free-flowing powders, had HR above 1.5, while powders with minimal interparticulate friction, have ratios of less than 1.2. Carr created a further indirect technique for calculating powder flow from bulk densities. According to Eq. 3 and 5, the percentage compressibility of a powder is a direct indicator of the possible strength and stability of a powder arch. Cumulatively, based on powder flow classification, higher Carr's index connotes higher HR values and lower powder flow.

In Figure 6 and Figure 7, Carr's index and HR were each compared with the static angle of repose (α_s), respectively.

The angle at which a powdery mass stops flowing is called the angle of repose. The avalanche angle, or the angle at which a stationary powder will start to flow, is a complementary property to (α_s). Even with high angles in the powder pile, a free-flowing powder will continue to flow. The gravitational force that moves the powder will, however, be lessened by reducing the pile angle. The attractive and frictional forces present within the powder balance out the gravitational force that was causing the flow at the point where the powder stops (Beakawi Al-Hashemi & Baghabra Al-Amoudi, 2018). The angle of repose of the experimental coprocessed diluents ranged from 14.02 to 30.81° which according to the USP powder classification connotes excellent powder flow. Both Carr's index and HR positively correlates with the static angle of repose. In both cases similar higher correlation coefficient and adjusted coefficient of determination values were obtained.
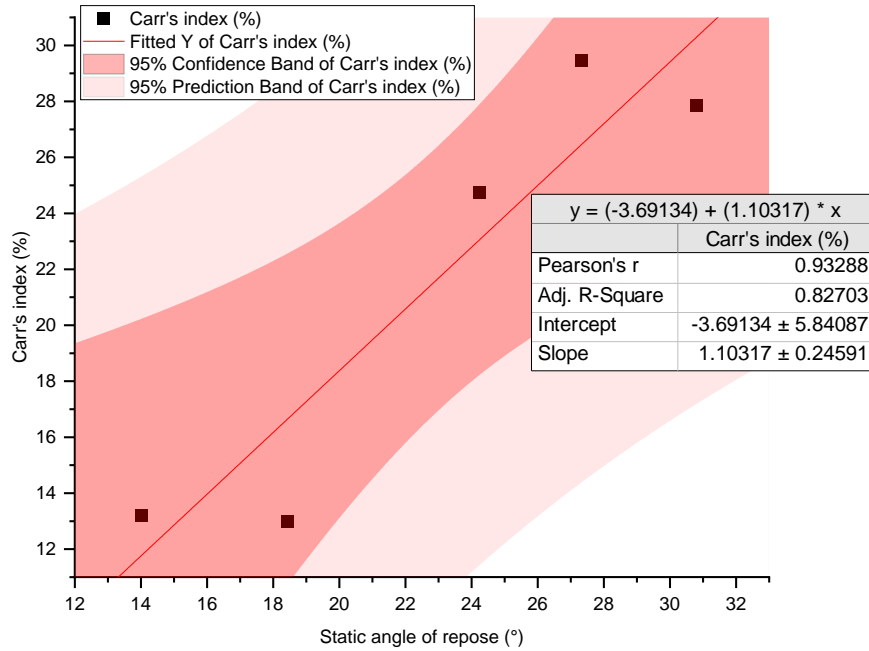
Figure 6: Correlation Carr's index and static angle of repose. The linear fit is indicated by the straight line followed by 95% confidence and prediction bands, respectively.
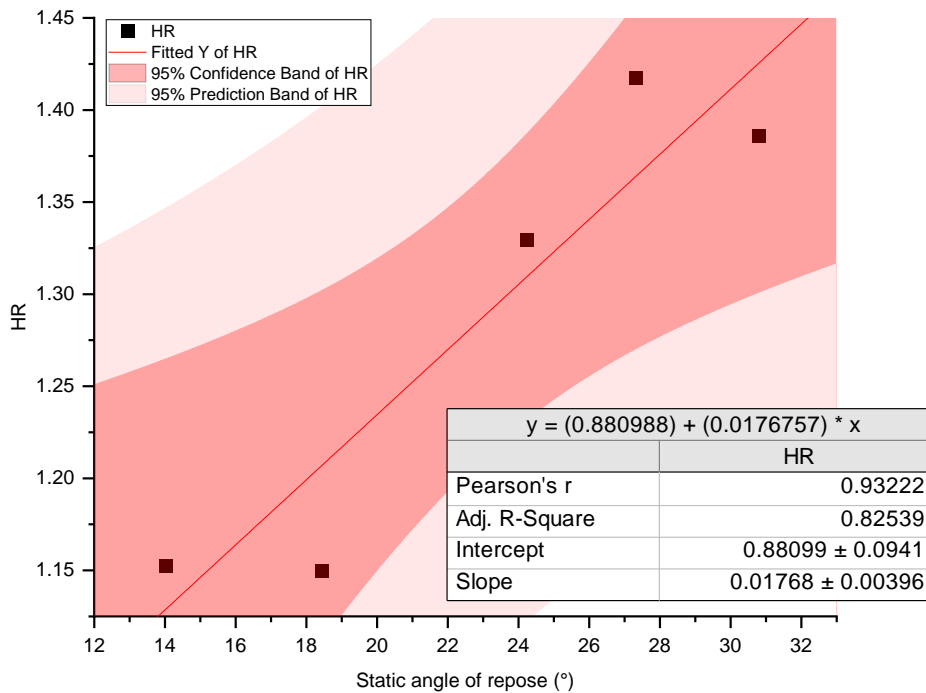
Figure 7: Correlation Hausner's ratio (HR) and static angle of repose. The linear fit is indicated by the straight line followed by 95% confidence and prediction bands, respectively.
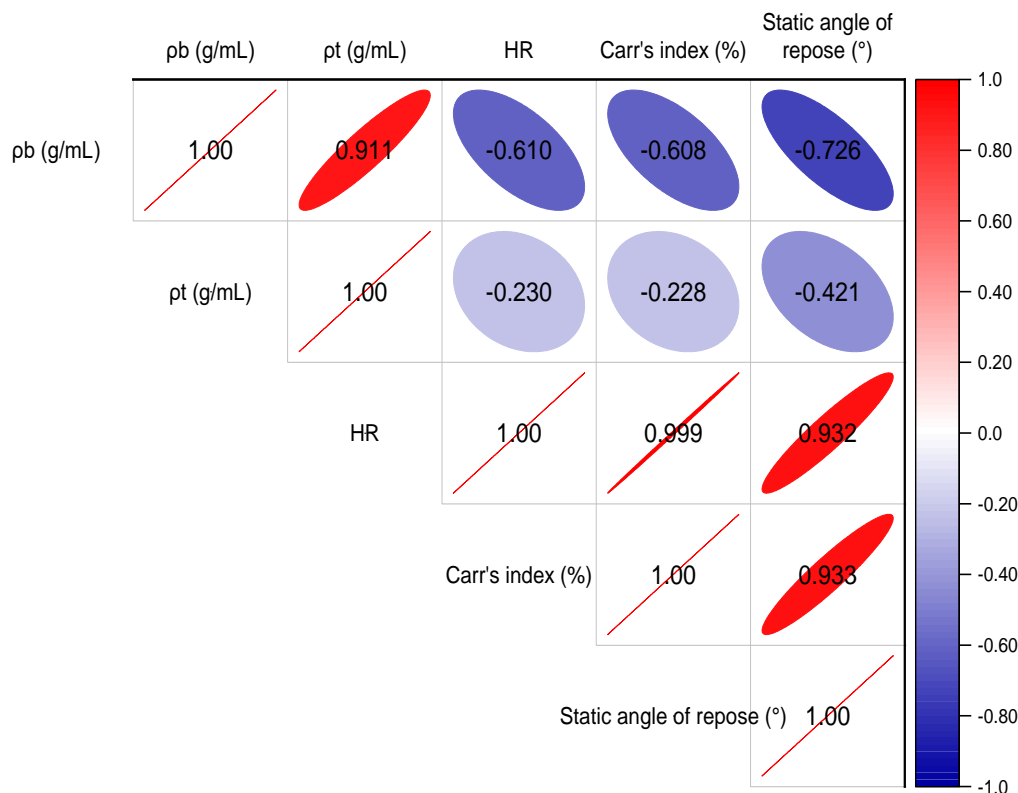
Figure 8: Correlation matrix representing modulus of Pearson product moment correlation coefficient represented by the colour, size and orientation of the ellipse. With positive correlation (red colour), the ellipse tilts forward and the converse holds for negative correlation (blue colour). The broader the ellipse, the lesser the strength of the correlation, while narrower bands depict stronger correlation. In this Figure, all the negative correlations were not statistically significant.

95% confidence band and 95% prediction band
The confidence band around all the fitted regression lines in Figure 3-7 display the upper and lower bounds of every feasible fitted line for the provided data for the selected confidence level (95%). In other words, there is a 95% chance that the best-fit line falls inside the confidence intervals. On the other hand, the range of values within which $100(1-\alpha)$ % of all experimental points in a set of repeated measurements are anticipated to fall is known as the prediction band for the chosen confidence level $(1-\alpha)$. The default value of α is 0.05. The probability that an anticipated data point will fall inside a prediction band with $(1-\alpha) =0.95$ is 95%. In other words, there was a 95% probability that if one more experiment data point whose independent variable is within the independent variable range of the original dataset is included, the data point will appear inside the prediction band (Crowder et al., 2020; Moser, 1996).

Correlation matrix and ellipse plot
To visually analyse correlation in simple linear fitting, ellipse plots were utilized. The two variables X and Y were assumed to have a bivariate normal distribution when doing linear regression. This distribution has a bell-shaped surface and is a co-effect of (X, Y). For a particular level of confidence, such as 95%, it could be deduced that 95% of the variable pairs (x, y) will fall inside the confidence area covered by the upper ellipse, and the projection of the confidence area on the XY plane is the confidence ellipse for prediction(Crowder et al., 2020). The same concept was used in the confidence ellipse for the population mean, which only displays the confidence ellipse of the mean $(\bar{x}, \bar{y})$. The correlation coefficient, r, controls the ellipse's appearance. As could be noted in Figure

8, the correlation matrix of the entire dataset was presented to give a holistic description of the correlations between the powder test methods(Moser, 1996). The modulus of Pearson's product moment correlation coefficient was represented by the colour, size and orientation of the ellipse. With positive correlation (red colour), the ellipse tilts forward and the converse holds for negative correlation (blue colour). The broader the ellipse, the lesser the strength of the correlation, while narrower bands depict stronger correlation. The Pearson correlation scale was also represented alongside the matrix plot. The value of r typically resonates from -1 through 0 to + 1. As the value of r approaches the extremes, the correlation between the bivariate variables get stronger in either the positive or negative direction (Mohr et al., 2022). The neutral value of 0 shows lack of linear association. In this way, we could have an inferential appreciation of the relationships between the test methods and better representation of the true powder behaviour compared to the earlier descriptive presentation (Figure 2). For brevity, the matrix could be interpreted across the rows and columns. From the first row, bulk density strongly correlates with tap density in the positive direction (r=+0.911), however it slightly correlates negatively with HR (r=-0.610), Carr's index r= (-0.608), and static angle of repose (r=-0.726). However, the latter correlations were not significant, statistically. From the second row, tap density also shows a non statistically significant negative correlation with HR (r=-0.230), Carr's index (r=-0.228), and static angle of repose (r=-0.421). In the third row, the strong positive correlation modulus of HR with Carr's index (r=+0.999) and static angle of repose (r=+0.932) were evident. Finally, in the fourth row,

Carr's index strongly correlated with static angle of repose ($r=+0.933$).

In all the bivariate correlations in the matrix Figure 8, the correlation coefficients corroborate the Pearson's r in the regression plots in Figure 3-7 which signifies mutual concordance between the simple linear fitting and the correlation statistics in terms of magnitude and direction. However, the slight variation the exact correlation coefficient values between Figure 3-7 and Figure 8 could be attributable to statistical methods of estimation and approximation of the standard errors and residuals in the fitting algorithm.

CONCLUSION

Simple linear regression modelling of bivariate powder flow datasets has provided a powerful but simplistic statistical relationship for characterizing the modulus of association between Hausner's ratio, Carr's index, and static angle of repose of the model excipients. While the descriptive association between the powder flow metrics in the tabulated data and parallel coordinate plots lack any practical significance, the correlation matrix alongside the linear regression plots provided reliable and robust means of expressing the relationships between the test methods.

ACKNOWLEDGEMENT

REFERENCES

Alderborn, G., & Frenning, G. (2017). Tablets and compaction. In M. Aulton & K. M. G. Taylor (Eds.), *Aulton's Pharmaceutics: The Design and Manufacture of Medicines* (5th ed., pp. 517–563). Elsevier.

Amidon, G. E., Meyer, P. J., & Mudie, D. M. (2017). Particle, powder, and compact characterization. In *Developing Solid Oral Dosage Forms: Pharmaceutical Theory and Practice: Second Edition* (pp. 271–293). Elsevier Inc. https://doi.org/10.1016/B978-0-12-802447-8.00010-8

Angelini, C. (2019). Regression Analysis. *Encyclopedia of Bioinformatics and Computational Biology: ABC of Bioinformatics*, *1–3*, 722–730. https://doi.org/10.1016/B978-0-12-809633-8.20360-9

Armstrong, N. A. (2007). Tablet Manufacture by Direct Compression. In J. Swarbrick (Ed.), *Encyclopedia of Pharmaceutical Technology* (3rd ed., Vol. 6, pp. 3673–3683). Informa Healthcare Inc.

Beakawi Al-Hashemi, H. M., & Baghabra Al-Amoudi, O. S. (2018). A review on the angle of repose of granular materials. *Powder Technology*, *330*, 397–417. https://doi.org/10.1016/J.POWTEC.2018.02.003

Bulk Density and Tapped Density of Powders | USP. (n.d.). Retrieved May 4, 2021, from https://www.usp.org/harmonization-standards/pdg/general-chapters/bulk-density-and-tapped-density-of-powers

Crowder, S., Delker, C., Forrest, E., & Martin, N. (2020). Determining Uncertainties in Fitted Curves. *Introduction to Statistics in Metrology*, 227–265. https://doi.org/10.1007/978-3-030-53329-8_10

Goh, H. P., Heng, P. W. S., & Liew, C. V. (2018). Comparative evaluation of powder flow parameters with reference to particle size and shape. *International Journal of Pharmaceutics*, *547*(1–2), 133–141. https://doi.org/10.1016/j.ijpharm.2018.05.059

Help Online - Origin Help - Algorithms (Linear Regression). (n.d.). Retrieved May 26, 2023, from https://www.originlab.com/doc/en/Origin-Help/LR-Algorithm#The_Linear_Regression_Model

Krantz, M., Zhang, H., & Zhu, J. (2009). Characterization of powder flow: Static and dynamic testing. *Powder Technology*, *194*(3), 239–245. https://doi.org/10.1016/J.POWTEC.2009.05.001

Lu, H., Bian, Y., Wang, Z., Guo, X., Liu, H., Cao, J., & Qu, K. (2023). Characterization of non-Newtonian rheological behaviors of powders. *Powder Technology*, *417*, 118281. https://doi.org/10.1016/J.POWTEC.2023.118281

Marchetti, L., & Hulme-Smith, C. (2021). Flowability of steel and tool steel powders: A comparison between testing methods. *Powder Technology*, *384*, 402–413. https://doi.org/10.1016/J.POWTEC.2021.01.074

Mohr, D. L., Wilson, W. J., & Freund, R. J. (2022). Linear Regression. *Statistical Methods*, 301–349. https://doi.org/10.1016/B978-0-12-823043-5.00007-2

Moser, B. K. (1996). The General Mixed Model. *Linear Models*, 177–188. https://doi.org/10.1016/B978-012508465-9/50010-7

Ostertagová, E. (2012). Modelling using Polynomial Regression. *Procedia Engineering*, *48*, 500–506. https://doi.org/10.1016/J.PROENG.2012.09.545

Pérez, P., Suñé-Negre, J. M., Miñarro, M., Roig, M., Fuster, R., García-Montoya, E., Hernández, C., Ruhí, R., & Ticó, J. R. (2006). A new expert systems (SeDeM Diagram) for control batch powder formulation and preformulation drug products. *European Journal of Pharmaceutics and Biopharmaceutics*, *64*(3), 351–359. https://doi.org/10.1016/j.ejpb.2006.06.008

Rojas, J., Buckner, I., & Kumar, V. (2012). Co-proccessed excipients with enhanced direct compression functionality for improved tableting performance. In *Drug Development and Industrial Pharmacy* (Vol. 38, Issue 10, pp. 1159–1170). https://doi.org/10.3109/03639045.2011.645833

Salehi, H., Barletta, D., & Poletto, M. (2017). A comparison between powder flow property testers. *Particuology*, *32*, 10–20. https://doi.org/10.1016/J.PARTIC.2016.08.003

Salim, I., Kehinde, O. A., Abdulsamad, A., Khalid, G. M., & Gwarzo, M. S. (2018). Physicomechanical Behaviour of Novel Directly Compressible Starch-MCC-Povidone Composites and their Application in Ascorbic Acid Tablet Formulation. *British Journal of Pharmacy*, *3*(1), 527. https://doi.org/10.5920/BJPHARM.2018.03

Salim, I., Olowosulu, A. K., Abdulsamad, A., Gwarzo, M. S., Khalid, G. M., Ahmad, N. T., Eichie, F. E., & Kurfi, F. S. (2021). Application of SeDeM Expert System in the development of novel directly compressible co-processed excipients via co-processing. *Future Journal of Pharmaceutical Sciences 2021 7:1*, *7*(1), 1–12. https://doi.org/10.1186/S43094-021-00253-Z

Twitchell, A. M. (2018). Mixing. In M. E. Aulton & K. M. Taylor (Eds.), *Aulton's Pharmaceutics: The Design and Manufacture of Medicines* (5th ed., pp. 172–188). Elsevier.

United States Pharmacopoeia. (2015). *<616> Bulk and tap densities of powders*.

Wang, K., & Sun, C. C. (2021). Direct compression tablet formulation of celecoxib enabled with a pharmaceutical solvate. *International Journal of Pharmaceutics*, *596*, 120239. https://doi.org/10.1016/J.IJPHARM.2021.120239